Changes in Arrangement of Lamella and Fine Crystallite in Fluorinated "Crystalline" Transparent Fibers with Drawing

Atsuhiro Fujimori* and Yuichiro Hayasaka

Graduate School of Science and Engineering, Yamagata University, Yonazawa, Yamagata, 992-8510, Japan

Received April 10, 2008; Revised Manuscript Received July 21, 2008

ABSTRACT: Recently, we developed a "crystalline" plastic optical fiber with excellent heat resistance and dimensional stability. For the practical use of this crystalline optical fiber in the near future, an accurate control of the solid-state structure is indispensable because of the necessity of reducing light refraction at the crystalline/amorphous interface. In the present study, changes in the fine structure and lamella arrangement upon drawing poly[tetrafluoroethylene-*co*-(perfluoroethylvinylether)] (abbrev. EFA) transparent crystalline fibers were investigated by using wide-angle X-ray diffraction (WAXD) and small-angle X-ray scattering (SAXS) methods. The EFA was crystallized as a lamella crystal in the fibers and formed a thicker lamella (thickness: at least 27 nm). This polymer might form a "switchboard-type" lamella. Upon the drawing of the EFA fibers, four-point SAXS diagrams developed in the photograph, which implied that a particular type of layer structure, an alternately tilted lamella arrangement known as the herringbone, was formed. Moreover, the previously proposed packing mode of general fluorinated polymers was required to be modified from quasi-hexagonal to orthorhombic in a reciprocal lattice in order to assign all reflective indexes.

1. Introduction

Partially crystalline polymers usually have both crystalline and amorphous regions. It is well-known that crystalline polymers construct hierarchical structures ranging from lamellae on the nanometer scale to spherulite on the mesoscopic scale.[1−3] The polymer crystals in these crystalline polymers are generally formed by the folding of the main chain. In many cases, since both inter- and intraspherulite chains form the amorphous region, crystalline polymers are essentially intermingled states of the crystalline and the amorphous regions. Therefore, crystalline polymers are not suitable candidates for use in plastic optical fibers (POFs) because of the occurrence of light refraction at the crystalline/amorphous interface. The amorphous POFs lack heat resistance and dimensional stability.

However, if the construction of extremely homogeneous crystalline POFs is realized, "crystalline" POFs with excellent heat resistance and dimensional stability can be developed. The heat-resistant POFs will efficiently demonstrate their optical ability in a circuit exposed to a high temperature of more than 125 °C; so far there have been no products of heat-resistant POFs that can sustain temperatures higher than 125 °C. If the heat-resistant POFs are realized, light wiring in automobiles will also be achieved; the heat-resistant POFs will not only connect the AV equipment but also connect the control system around the engine. As a result, the overall body of an automobile will become lighter. This future technology is based mainly on "crystalline fluorinated polymers" having a high crystallinity. Generally, polytetrafluoroethylene (PTFE; $-(CF_2-CF_2)_n-$) and its copolymers easily form rigid helices in order to yield extended-chain crystals (ECC). This ECC structure of 13/6 helical conformation for PTFE is different from both planar zigzag polyethylene[4] and 3/1 helical polypropylene chains.[5] Therefore, It seems especially difficult for PTFE to form a lamella structure because of its rigid molecular chain.[5−10] In addition, since tetrafluoroethylene copolymers obtained by the incorporation of several comonomers exhibit extremely fast crystallization rates,[11] their spherulites generally cannot be observed until they are sufficiently large. Therefore, PTFE exhibits a high degree of crystallinity of over 90%.[12−14]

Poly[tetrafluoroethylene-*co*-(perfluoroalkylvinylether)] ($-[(CF_2-CF_2)_n-(CF(OCF_2CF_3)-CF_2)]_m-$, abbrev. EFA (alkyl = ethyl) or PFA (alkyl = propyl))[15] has a unique role in the plastics industry due to its inertness, heat resistance, and low coefficient of friction in a wide temperature range. Generally, fluorinated compounds and fluoropolymers have excellent chemical resistance, oil resistance, and oil- and water-shedding resistance.[16−19] They have been used as rubbers at high temperatures and in several lubricating fluorine manufactured products.

However, in the field of fundamental science, structural studies on fluorinated polymers have progressed slowly since the time these polymers were first reported by Bunn and Howells in 1954.[20] We could find very few reports on systematic structural studies on PTFE or tetrafluoroethylene-based fluorinated copolymer because this compound forms the complicated 13/6 helical conformation, lack of solubility in organic solvents, too high values of melting point, crystallinity, and melt-viscosity, and the occurrence of a poisonous gas in the case of decomposition.[6,8]

Further, although EFA is a crystalline polymer, processed EFA samples that have a high crystallinity are as transparent as amorphous polymers such as polymethymethacrylate (PMMA)[21] and polyacrylic acid (PAA), as shown in Figure 1. This experimental fact is not well-known. Probably, since the transparency of organic materials depends on the existence of differences in electron density between the crystalline and the amorphous regions, it is considered that a high crystallinity of EFA relates closely to the occurrence of transparency. Additionally, processed EFA tubes break into pieces just like glass tubes when an excessive bending force is applied upon them. It is obvious that the enhancement of these unique properties of the processed EFA fibers is a result of the changes in the crystal structure and crystalline morphology of EFA fibers that take place during the drawing process. Further, fluorinated polymers do not absorb infrared light because of their stretching vibration and a lack of C−H bonds.[22,23] Hence, a "crystalline" POF made by fluorinated polymers transports not only visible light but also infrared light.

In this study, the changes in the fine structure and lamella arrangement of the fibers formed by tetrafluoroethylene copolymers upon drawing are investigated by using wide-angle X-ray diffraction (WAXD) and small-angle X-ray scattering (SAXS)

* To whom correspondence should be addressed: Tel and fax: +81-238-26-3073. E-mail: fujimori@yz.yamagata-u.ac.jp.

10.1021/ma800801d CCC: $40.75
Published on Web 09/24/2008

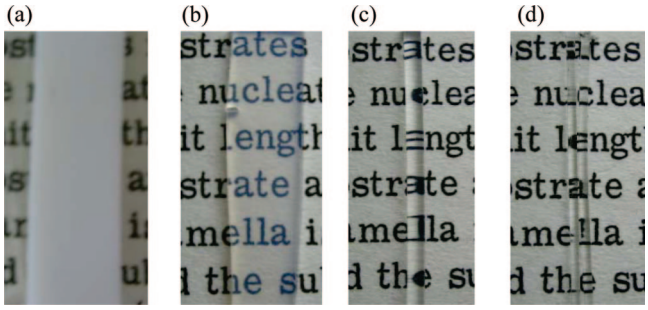

Figure 1. Changes in transparency of several processed materials of "crystalline" fluorinated copolymers: (a) bulk EFA, (b) pressed-processing sheet, (c) crystalline fiber with drawn ratio = 3, (d) crystalline fiber with drawn ratio = 5.

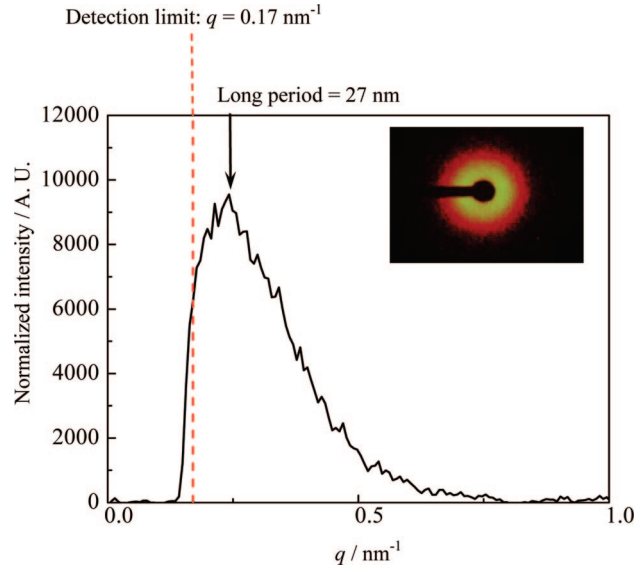

Figure 2. SAXS pattern and profile of undrawn EFA "crystalline" fiber at room temparture. (The dashed line is detection limit in this study.)

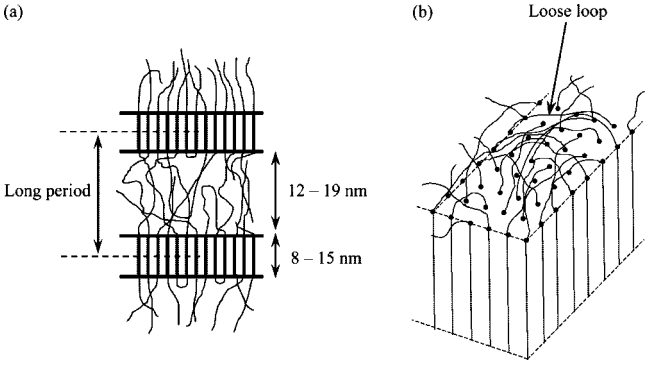

Figure 3. Schematic illustrations of "switchboard-type" lamella models of fluorinated copolymers like an EFA (a) along the *c*-axis, and (b) in an $a-b$ plane.

methods. We have found very few reports on the studies on the structural changes in fluorinated polymers upon drawing, whereas there are many reports of studies on hydrocarbons. Therefore, this study may also be valuable as fundamental research in the field of polymer physics. In addition, we have discussed the relationships between the origins in order to elucidate the occurrence of transparency and structural changes in molecular arrangements.

2. Experimental Section

2.1. Materials. *2.1.1. Fluorinated Copolymer.* The fluorinated copolymers used in this study were provided by DuPont-Mitsui Fluorochemicals Co. Ltd. EFA is a random copolymer obtained from the copolymerization of tetrafluoroethylene $-(CF_2-CF_2)_n-$ and perfluoroethylvinylether $-(CF_2-CF(OCF_2CF_3))_n-$. The amount of comonomers of these materials was about 7 wt %. In the bulk state, side-chain parts formed by comonomers cannot be incorporated into the crystal part in lamellar. The molecular weight of the EFA processed to a crystalline fiber form was about 600,000. This molecular weight was examined by a computer simulation on the basis of the viscoelasticity of the fiber in a molten state because it is difficult to dissolve these polymers in an organic solvent.

2.1.2. Drawing of EFA Fibers. EFA fibers were drawn uniaxially by using a hand-drawing apparatus in an air oven at 280 °C. The surface of the fiber specimen was marked at intervals of 2 mm in order to measure the draw ratios. The drawing speed was fixed at 20 mm/min, and the fiber was annealed at 280 °C for 3 min before drawing. In order to attain the constant condition, EFA fibers were cooled by immersing into the water after drawing. Using this method, we obtained fibers with excellent transparency (Figures 1(c) and 1(d)).

2.2. Experimental Methods. *2.2.1. Small-Angle X-ray Scattering (SAXS).* The crystalline morphology of the drawn EFA copolymers was characterized with a SAXS instrument (M18XHF, MAC Science Co.) consisting of an 18 kW rotating-anode X-ray generator with a Cu target (wavelength, $\lambda = 0.154$ nm) operated at 50 kV and 300 mA.[24] This instrument comprised a pyrographite monochromator, pinhole collimation system ($\phi \sim 0.3$, 0.3, and 1.1 mm), vacuum chamber for the scattered beam path, and a two-dimensional imaging plate detector (DIP-220). The sample-to-detector distance was adjusted to 710 mm. The exposure time for each sample was 30 min. For the SAXS measurements, each sample (thickness: approximately 0.5 mm) was placed in a sample holder so that its position remained unchanged. The theoretical detection limit of the SAXS measurement in this study almost corresponded to the value of $q = 0.128$ nm^{-1} estimated by using the camera distance (from sample to the imaging plate) in the apparatus. However, the actual detection limit examined by counting the pixel numbers of enlarged SAXS patterns on the monitor of an analytical computer was $q = 0.170$ nm^{-1} (dashed line in the profile of Figure 2). Hence, the observable maximum value of the long period between the centers of gravity of the lamellae in this study was 36.9 Å.

2.2.2. Wide-Angle X-ray Diffraction (WAXD). In order to obtain the WAXD data for the drawn fibers, an *R*-axis diffractometer (Rigaku Co.) was operated at 45 kV and 200 mA to generate Cu Kα radiation ($\lambda = 0.1542$ nm). WAXD photographs of the samples were taken at room temperature by using a graphite monochromator and a 0.3 mm pinhole collimator. Diffraction data were recorded on a cylindrical imaging plate detector equipped with an interface to a computer system. The camera length was 127.4 mm, and the exposure time was 600 s.

2.2.3. Differential Scanning Calorimetry (DSC). Thermal analyses were carried out by using a Seiko Instruments model DSC200 differential scanning calorimeter (DSC). The DSC measurements were performed at a standard scanning rate of 10.0 °C min^{-1}. A sample mass of *ca.* 5.00 mg was used for all the DSC measurements. As usual, the scanning of DSC measurements and the heating and cooling cycle were repeated twice in order to examine the difference between the peak position and transition enthalpy in the first and second heating.

3. Results and Discussion

3.1. Changes in Lamella Arrangement of Transparent "Crystalline" EFA Fiber. Figure 2 shows the SAXS pattern and normalized one-dimensional SAXS profiles, where q is the scattering vector ($q = 4\pi \sin\theta/\lambda$; θ = Bragg angle), of the undrawn transparent crystalline EFA fiber at room temperature. A ring-shaped SAXS pattern was observed, which indicated the

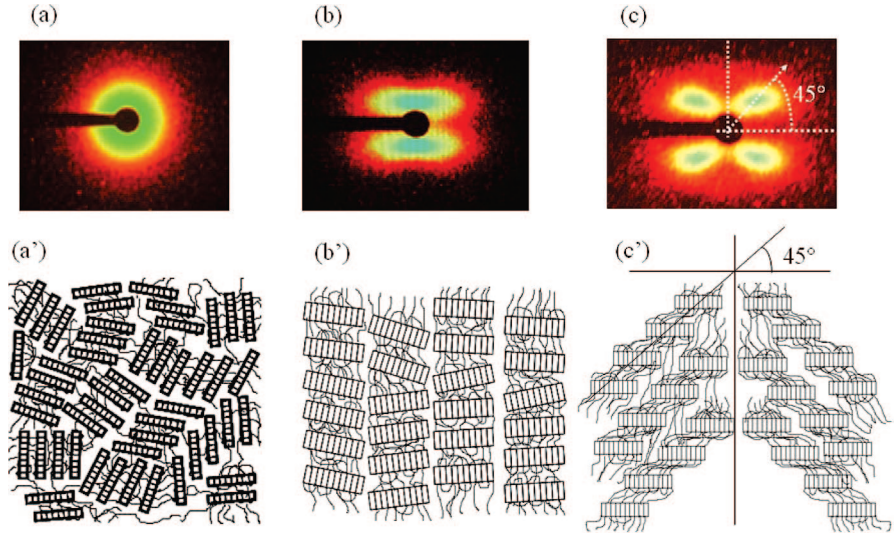

Figure 4. Changes in SAXS patterns and corresponding lamella arrangement models of EFA transparent "crystalline" fiber with drawing; (a), (a′) undrawn, (b), (b′) 3 times, and (c), (c′) 5 times drawing.

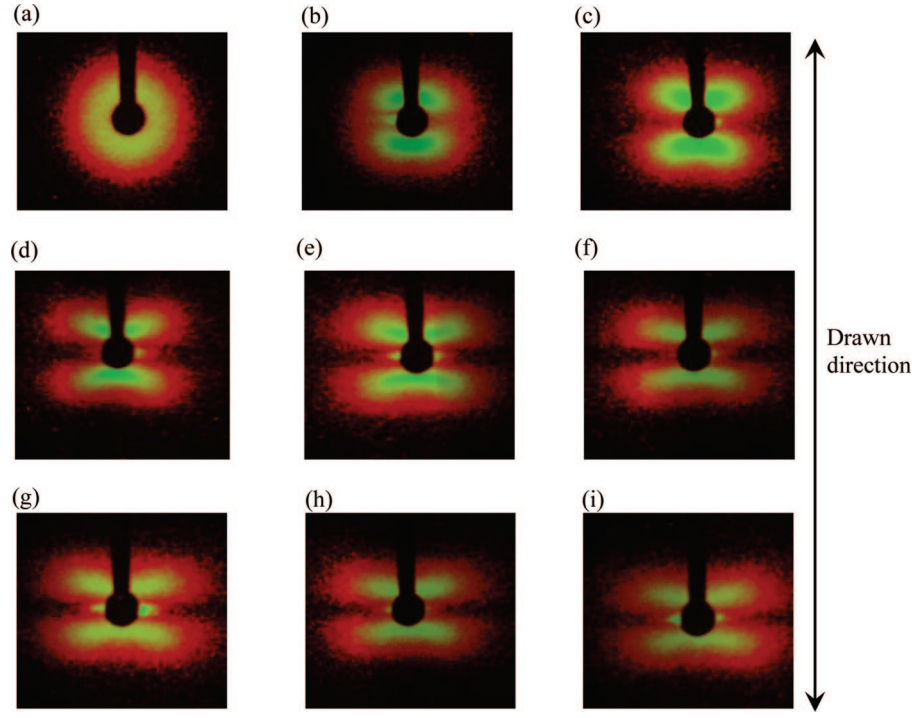

Figure 5. Changes in SAXS patterns of EFA "crystalline" transparent fibers with drawing at a ratio of (a) 1.0, (b) 1.5, (c) 2.0, (d) 3.0, (e) 4.0, (f) 5.0, (g) 6.0, (h) 7.0, and (i) 8.0.

formation of an isotropic random micellar texture. It was found that the tetrafluoroethylene copolymer formed lamella structures since the undrawn EFA used in this study exhibited isotopic SAXS patterns. The long period of the undrawn sample was estimated to be 27.0 nm. A high-crystallinity EFA sample formed relatively thicker lamellae than the general hydrogenated crystalline polymers. On the contrary, the SAXS pattern of previous reported PTEF was obscure, and the corresponding profile exhibited extremely low intensity because this polymer almost formed an extended chain and not micellar or lamellar structure.[25]

On the basis of the results of the SAXS measurements of the undrawn EFA fiber, we suggested the following lamella model for tetrafluoroethylene copolymers. According to A. Keller's suggestion,[1] it was assumed that general crystalline polymers form a regular sharp hold. However, the tetrafluoroethylene copolymers used in this study did not form an arrangement of these adjacent reentries because of the existence of a rigid molecular chain and a lack of flexibility. It seemed that the folded parts formed in the ether bond-rich region within the fluorinated main chain. However, so many perfluoroalkylvinylether units could not have contributed to the formation of the folded parts because the ratio of the absolute amounts of the comonomers was extremely low. Hence, we proposed a "switchboard-type" lamella model of these tetrafluoroethylene copolymers, shown in Figure 3, according to P. J. Flory's suggestion.[25,26] In this case, it was supposed that there existed a relatively large amorphous region because of the existence of the large long-period structure estimated by SAXS. From the qualitative estimation of the lamella thickness based on the crystallization degree obtained from the DSC measurements, the thickness of the crystalline regions of the EFA lamella form

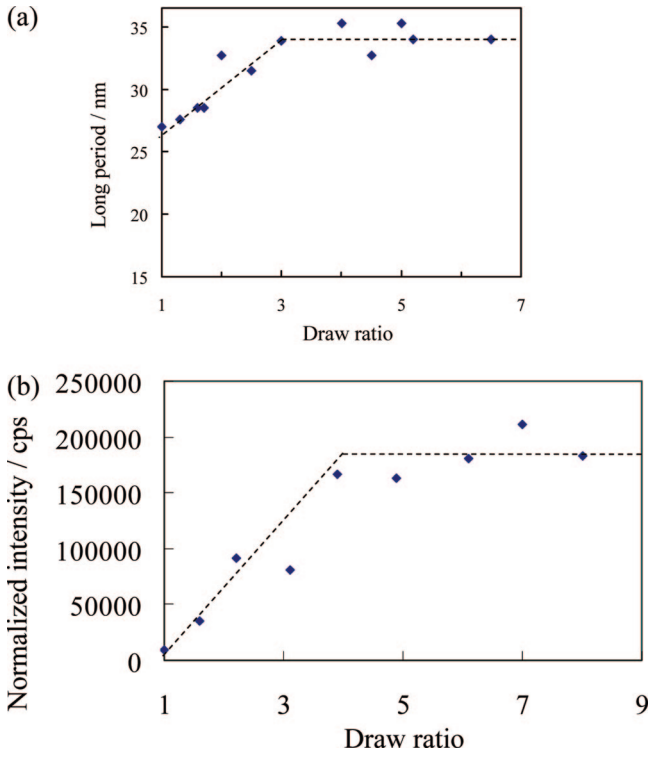

Figure 6. Plots of draw ratio vs (a) long periods and (b) normalized intensity estimated by SAXS measurements of EFA "crystalline" transparent fibers.

was estimated to vary within a range from 6 to 16 nm (as calculated by using the fusion enthalpy of as-polymerized PTFE, ΔH_{endo} (58.4 J/g), as the standard fusion enthalpy of EFA, $\Delta H_{endo,0}$.[25] The existence of the thick amorphous layer (over 10 nm) also supports the validity of our proposed switchboard-type lamella model.

Figure 4 shows the SAXS patterns and corresponding micellar or lamellar arrangement models[27−29] for DR1 (draw ratio = 1.0, undrawn), DR3, and DR5 transparent crystalline fibers of EFA. It is necessary to pay attention to easy connection between scatting patterns and lamellar models because the scatting data as well as X-ray diffraction data allow the existence of various structures (such as existence of void, differences in crystal densities, and so on). Therefore, scattering patterns in this study are carefully analyzed following much previous literature in this field. A ring-shaped SAXS pattern was observed for the undrawn DR1 sample (Figure 4 (a)), while two- or four-point patterns were observed for the DR3 (Figure 4 (b)) or DR5 (Figure 4 (c)) fiber samples. The former indicated a random micellar texture (Figure 4 (a′)), and the latter indicated some lamella structures oriented with respect to the draw direction. The appearance of the two-point SAXS patterns implied the formation of an arrangement of lamellae parallel to the draw direction (Figure 4 (b′)). As the fiber was drawn further, the interlamella and/or intralamella slips probably occurred, forming the small kink bands in the lamellae. The slip angle of the interlamellae was 45° as calculated by using the position of the strongest spot in the SAXS picture. In accordance with the changes in lamellae, the grain boundaries or amorphous parts between two neighboring lamellae were also distributed regularly toward the draw direction, and they thus resulted in a periodic change in density in the direction normal to them, which accounted for the four-point diffraction pattern. That is, with an increase in the elongation of the EFA sample, a particular kind of layer structure, an alternately tilted lamella arrangement known as the herringbone, was formed inside the fibers (Figure 4 (c′)). Similar results were obtained in the case of drawn polyethylene

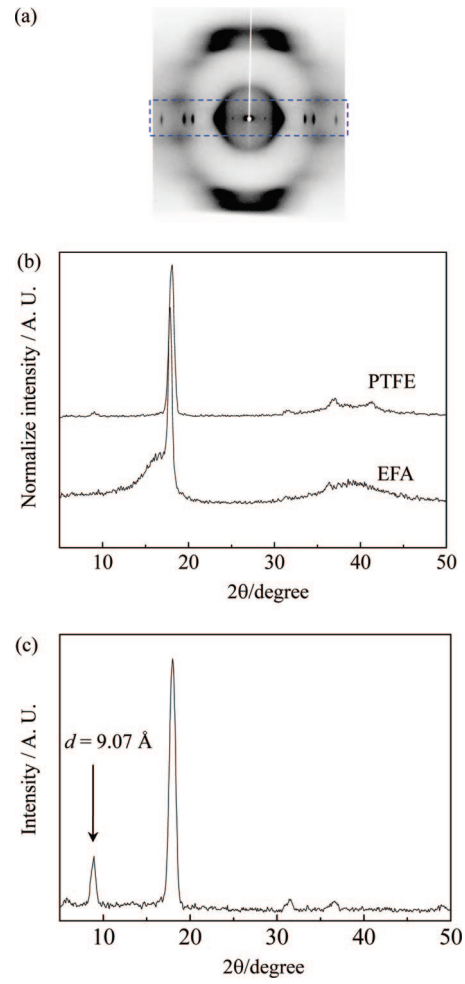

Figure 7. (a) WAXD patterns of "crystalline" transparent fibers of EFA at draw ratio = 8. (b) Comparison of WAXD profiles of EFA to PTFE. (c) WAXD profile of PTFE orientated rod formed by isostatic extrusion.

(PE) or polyacrylonitrile (PAN) fibers previously.[30−33] The long periods or interplanar spacings were calculated to be 33.9 and 35.3 nm for DR3 and DR5, respectively. These values were larger than the interplanar spacing of the undrawn sample (27.0 nm). This feature of the long periods corresponded well with that of PE, polypropylene (PP), and polyester.[30−37] From the viewpoint of enhancing transparency by using the drawing process, EFA fibers exhibited the elongation of the amorphous region with an increase in density in this region and indicated a resultant increase in the long period upon drawing.

Figure 5 shows the change in SAXS patterns upon drawing. SAXS patterns remained essentially unchanged even upon carrying out the drawing process for five times. However, from the results of the examination of light conductivity in db/km units for EFA fibers using infrared light (at $\lambda = 850$ nm), most superior abilities were confirmed in the DR5 fibers, and their transmission ability was observed to decrease gradually upon drawing for over six times. Moreover, the drawn EFA fiber broke when the elongation equaled almost nine times the original value. Just before breaking, the color of the drawn EFA fiber became white because of the appearance of many microvoids and/or defects and the light dispersion caused by these voids and/or defects. In order to estimate the changes in lamella thickness and differences in electron density upon drawing, plots of the draw ratio vs long periods and normalized intensity of SAXS profiles are shown in Figure 6. The values of the long period saturated at about DR3, and the normalized intensity was almost constant from DR4 to DR8. That is, the increase in the

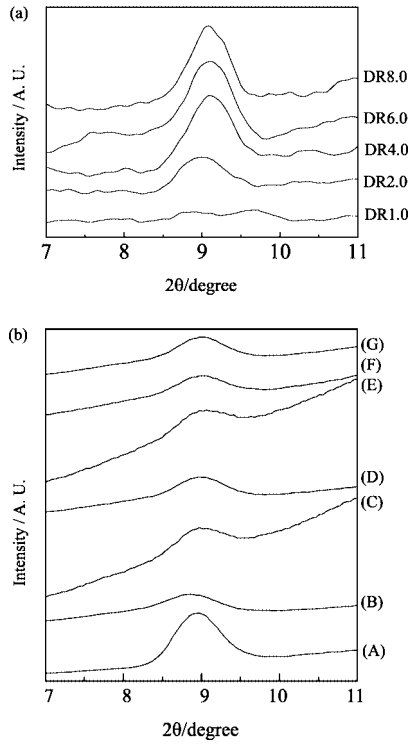

Figure 8. WAXD patterns of (a) drawn EFA transparent fibers, and (b) several fluorinated polymers in bulk: (A) PTFE, (B) FEP, (C) PFA, (D) PFA containing PTFE particle as nucleator, (E) low molecular weight EFA, (F) high molecular weight EFA, (G) EFA containing PTFE particle as nucleator.

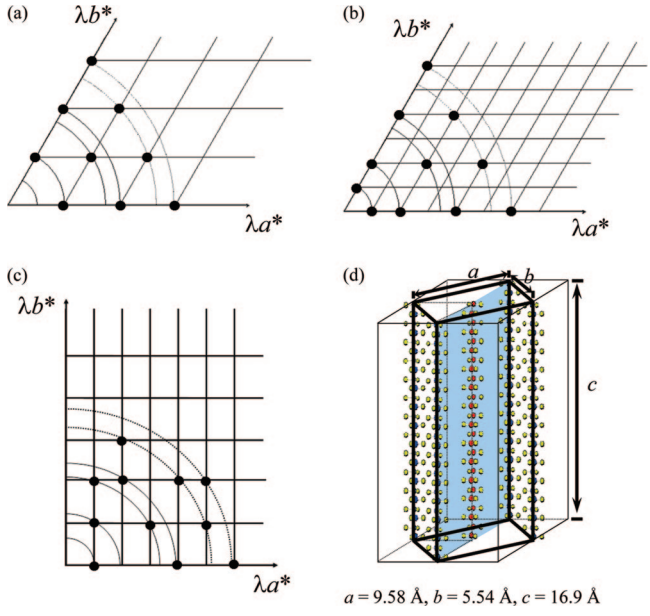

Figure 9. Reciprocal lattices of crystalline region for several fluorinated polymers (PTFE, EFA, and so on) represented by WAXD data: (a) previously reported quasi-hexagonal lattice, (b) a quasi-hexagonal lattice twice elongated a- and *b*-axis, (c) our proposed orthorhombic lattice, and (d) packing model of fluorinated chains in orthorhombic lattice.

lamella thickness containing an amorphous region stopped at DR3 (about 35 nm). After that, although the density of the amorphous region increased gradually upon drawing, a partial appearance of the voids might have occurred simultaneously. As a result, the difference in the overall density between the crystalline and the amorphous regions in the EFA fiber remained unchanged for a draw ratio of more than 4.

3.2. WAXD Study on Crystal Structure of Tetrafluoroethylene-Based Polymers. A typical example of the WAXD patterns for the drawn EFA fibers (DR8) is shown in Figure 7(a). Almost all spots existed on the equator line. Therefore, we have mainly discussed the WAXD profiles integrated along the equatorial direction in this section. Figure 7(b) shows a comparison of the WAXD profiles of the unoriented PTFE and the EFA samples. The lack of an amorphous curve around $2\theta = 15°$ was a peculiarity of the PTFE extended-chain crystal. A halo curve of the EFA appeared due to the existence of an amorphous region in the interlamella parts. However, the crystalline peak positions in both profiles were almost the same since the structure and main-chain arrangement in the crystalline region of EFA comprised repeating tetrafluoroethylene parts. That is, there was no difference between the structure of the crystalline region of PTFE and that of EFA.

Furthermore, most inner WAXD spots of an EFA fiber (Figure 7(a); the shadow next to the beam stopper) existed clearly when $2\theta = 9°$. These WAXD results included a very important result with regard to the fluorinated polymer crystal. The peak at around $2\theta = 18.0°$ in the WAXD profiles of tetrafluoroethylene and its copolymers was assigned to the (100) reflection in the quasi-hexagonal system according to the literature documented about 50 years ago.[20,38−40] Moreover, we could not find any reports related to the inner peak around $2\theta = 9°$. However, in the present WAXD profiles, small peaks at around $2\theta = 9°$ were confirmed and reproduced well by the high-power measurement using an X-ray diffractometer with an imaging plate as the detector. Further, in the WAXD profile of the oriented rod-shaped material processed by isostatic pressing of PTFE, this peak was clearly enhanced (Figure 7(c)). In addition, Figure 8 shows the changes in this peak in the WAXD profiles of the transparent crystalline EFA fiber upon drawing and the well-reproduced appearance of this peak in any type of fluorinated copolymers. From the result of Figure 8(a), it was found that the intensity of this peak around $2\theta = 9.0°$ increased gradually with an increase in the draw ratio. Figure 8(b) shows the WAXD profiles of several fluorinated copolymers such as PTFE, poly[tetrafluoroethylene-*co*-(hexafluoropropylene)] (FEP), PFA, PFA containing PTFE particles as nucleators, low molecular weight EFA (250,000), middle molecular weight EFA (300,000), and high molecular weight EFA (600,000) containing PTFE particles. All WAXD profiles of fluoropolymers used in this study contained this small peak at almost the same position. That is, this small peak around $2\theta = 9.0°$ reflected that the genuine crystal structure of fluorinated polymers was always confirmed in the WAXD profiles of tetrafluoroetthylene-based polymers. Furthermore, the intensity of this peak increased upon the formation of an orientated structure due to uniaxial drawing. However, no previous reports that confirm the presence of these small peaks exist, except for the paper we published last year.[25] It appears that the existence of this diffraction peak has been overlooked for about 50 years. In our previous report, we speculated that the peak at about $2\theta = 9°$ might correspond to the genuine (100) reflection.[25] In the present report, we clearly assert an interpretation of this peak and the crystal structure and partially modify our previous interpretation. In our previous paper,[25] we suggested that the previously reported lattice constant needed to be modified and the lengths of the *a*- and *b*-axes be doubled. In addition, the reflection at around $2\theta = 18.0°$ would be attributed to the (200) peak. If this did not occur, the reflective indexes of the small peaks at about $2\theta = 9°$ could not be determined. Figures 9(a) and 9(b) show the reciprocal lattice of PTFE and other perfluorinated copolymers observed along the *c*-axis under the suggestion that the parts forming the crystal region had the same structure for tetrafluoroethylene and tetrafluoroethylene copoly-

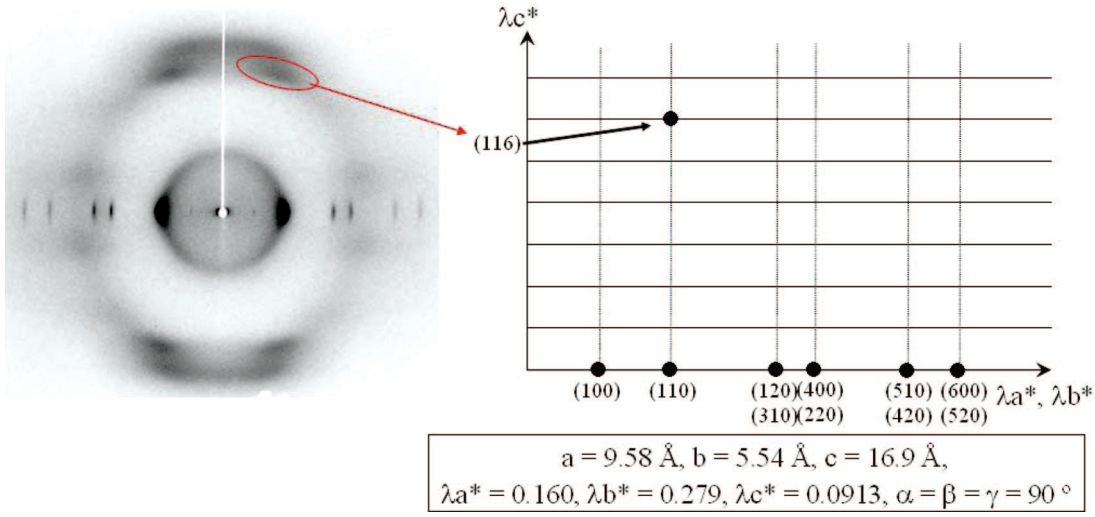

Figure 10. WAXD patterns and reciprocal lattice in the $\lambda b^*-\lambda c^*$ plane of crystalline region for EFA transparent fiber at DR5.

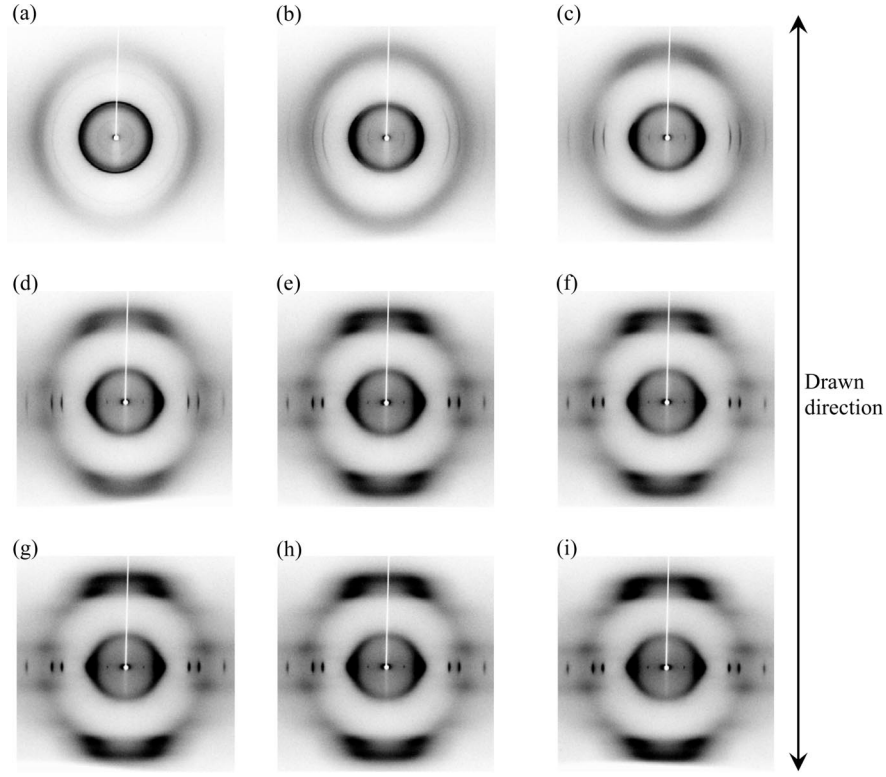

Figure 11. WAXD patterns of EFA transparent fiber at several drawing ratio at room temparture: (a) undrawn, (b) DR = 1.5, (c) DR = 2.0, (d) DR = 3.0, (e) DR = 4.0, (f) DR = 5.0, (g) DR = 6.0, (h) DR = 7.0, (i) DR = 8.0.

mers. The proposed lattice constant of PTFE[25] corresponded to $a = b = 11.08$ Å, $c = 16.8$ Å, $\alpha = 90°$, $\beta = 90°$, and $\gamma = 119.3°$ (Figure 6(b), quasi-hexagonal system) and improved upon the reports by Bunn, et al., Starkweather, Jr., et al., Clark et al.,[20,38−40] and other investigation groups (Figure 9(a), $a = b = 5.54$ Å, $c = 16.8$ Å, $\alpha = 90°$, $\beta = 90°$, and $\gamma = 119.3°$ (quasi-hexagonal system)). However, the reciprocal lattice of Figure 9(b) described a base-centered hexagonal lattice, whereas a base-centered lattice cannot exist in a group of hexagonal lattices. In addition, the reason for the appearance of a (100) reflection (peak at $2\theta = 9°$) weaker than a (200) one (peak at $2\theta = 18°$) was not clear. Therefore, we reproposed the necessity of modifying the lattice constant of tetrafluoroethylene and its copolymers in the present paper. We reconsidered the packing mode of fluorinated chains from a hexagonal to an orthorhombic system, as shown in Figures 9(c) and 9(d). In the reciprocal lattice in Figure 9(c), all WAXD reflection peaks confirmed in this study existed at a point of intersection in reciprocal lattice and all reflective indexes were decided. In this case, the peaks at $2\theta = 9°$ and 18° corresponded to the (100) and (110) reflection peaks, respectively. The lattice constants of this packing system were estimated to be $a = 9.58$ Å, $b = 5.54$ Å, and $c = 1.69$ Å ($\alpha = \beta = \gamma = 90°$). The hexagonal lattice essentially had the structural analogy of an orthorhombic one. In addition, the appearance of peaks at $2\theta = 9°$ and 18° was based on a different plane. Hence, the relation between intensities was not contradictory to an indexing rule. The three-dimensional packing model of the fluorocarbon chain in the

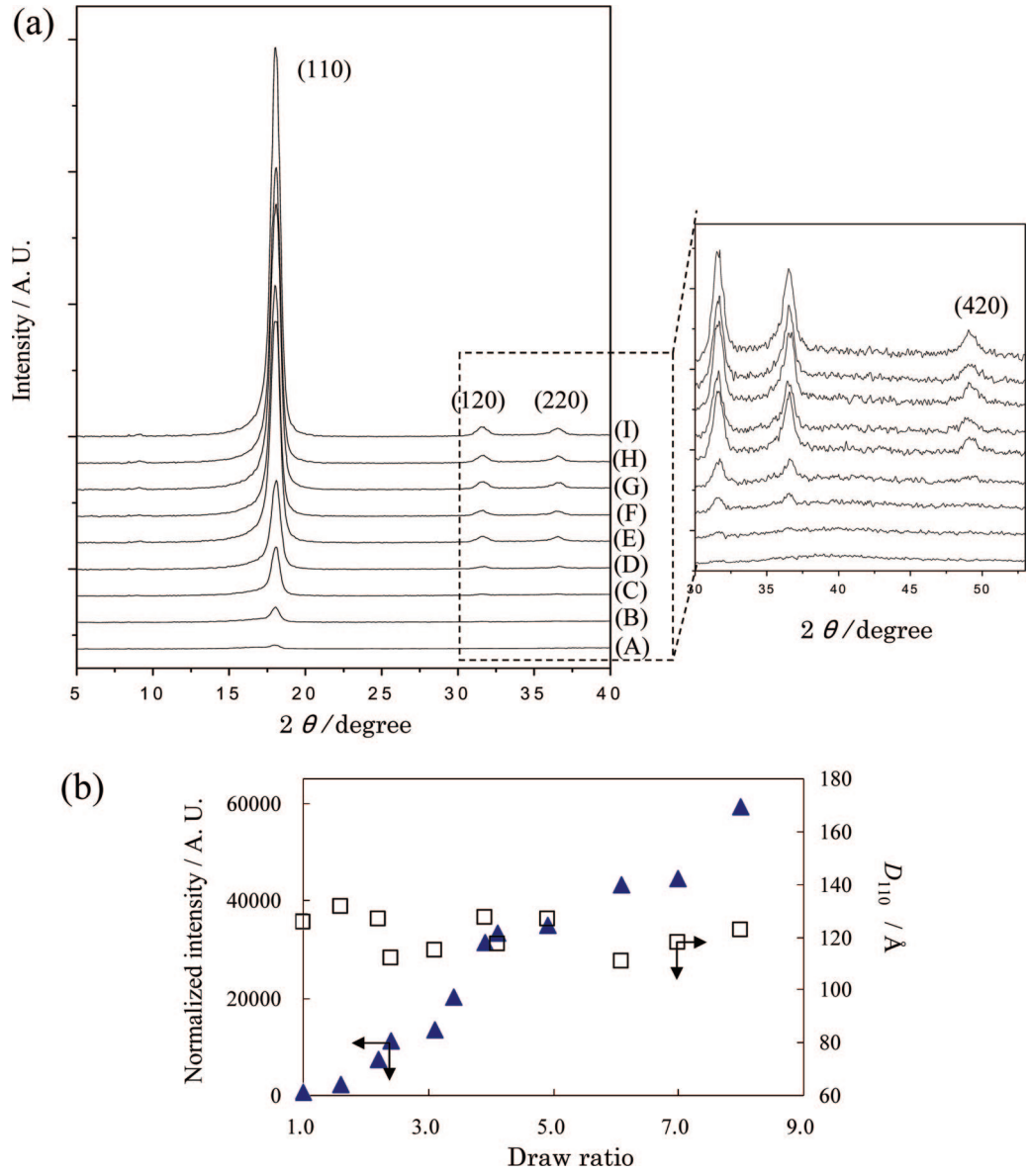

Figure 12. (a) WAXD profiles of EFA transparent fiber with drawing at room temparture: (A) undrawn, (B) DR1.5, (C) DR2.0, (D) DR3.0, (E) DR4.0, (F) DR5.0, (G) DR6.0, (H) DR7.0, (I) DR8.0. (b) Changes in normalized WAXD intensity and crystallite sizes with drawing estimated by Scherrer's formula.

crystalline region is shown in Figure 9(d). The validity of our proposed orthorhombic system of the crystalline fluorinated polymer was also supported by the estimation in a reciprocal lattice along the meridional direction. Figure 10 shows the possibility for applying an orthorhombic lattice to an index WAXD reflection spot along the meridional direction of the drawn EFA fiber at DR5. As mentioned above, we considered the EFA chains as an orthorhombic packing in the crystal region, and the highest diffraction peak in the profile was interpreted as a (110) reflection in this lattice in the following discussion.

3.3. Fine Structure Estimation of Transparent Crystalline EFA Fibers upon Drawing at Subnanometer Scales by WAXD. Figure 11 shows the WAXD patterns of the transparent EFA fiber at several drawing ratios. We can clearly see the gradual enhancement of the WAXD spots along the equator line upon drawing. From the viewpoint of one-dimensional profiles scanned along the equatorial direction, the peak intensity of (110), (120), (220), and (420) reflections in the orthorhombic lattice increased gradually with an increase in draw ratio (Figure 12(a)). The intensities of (110) peaks normalized by sample size and thickness linearly increased with drawn ratio, as observed from the plot of Figure 12(b) whereas the sizes of crystallite in the fiber estimated by Scherrer's formula[41] (diameter of crystallite along the normal direction to the (110) plane) are almost constant value all over the draw ratio. That is, it was considered that the increase in the crystallinity of the EFA fiber at the subnanometer scale rather related to increase of the lamellar thickness.

In order to evaluate the degree of orientation for the *c*-axis of the EFA crystallites along the draw direction, we calculated the orientation function (*f*) proposed by Hermans and coworkers[42] using the azimuthal WAXD profiles. The function *f* was defined as $f_\phi = (1/2)(3\langle\cos^2\phi\rangle - 1)$, $0 < f_\phi < 1$, where ϕ is the angle between the *c*-axis and the draw direction, and $\langle\cos^2\phi\rangle$ is obtained from the (110) and (120) azimuthal profiles by using Wilchinsky's procedure[43] (Figure 13(a)). Figure 13(b) shows the change in the orientation function of the EFA crystallites (f_ϕ) as a function of the draw ratio, where f_ϕ increased with the draw ratio up to DR = 2.5, after which it reached a saturation value of around 0.8. These findings suggested that

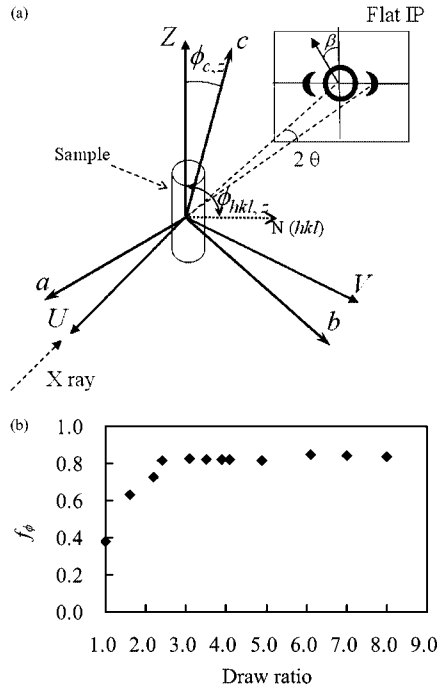

Figure 13. (a) Schematic representation of Wilchinsky method to estimate orientation coefficient of crystallite. (b) Plot of drawn ratio vs orientation coefficient of crystallite in EFA transparent fiber.

the orientation of an EFA crystallite in the fiber was complete at a draw ratio of 2.5. This value was almost the same as the draw ratio of the saturation value of a long period estimated by SAXS. That is, the orientation of the crystallite and the elongation of lamella reached constant values almost simultaneously. Then, the quasi-crystallization process by drawing progressed up to DR5, which was the saturation value of the normalized intensity estimated on the basis of the WAXD patterns. Judging from the draw ratio of the saturation of the SAXS intensity, the increase in the electron density of the amorphous region and the partial appearance of voids might be a simultaneous occurrence upon further drawing. The sample of the crystalline EFA fiber at DR5 was the most transparent and exhibited the highest conductivity of infrared light among all the drawn fibers used in this study. In conclusion, the functionality of light transmittance was closely related to the solid-state structure of the crystalline EFA fiber.

Figure 14(a) shows results of DSC measurements of EFA "crystalline" fibers at several drawn ratios in order to estimate crystallization degree and lamella thickness. Areas of melting peaks on thermograms related to fusion enthalpy are gradually increased with drawn ratios. Crystallization degree as calculated by using the fusion enthalpy of as-polymerized PTFE, ΔH_{endo} (58.4 J/g), as the standard fusion enthalpy of EFA, $\Delta H_{endo,0}$,[25] are plotted to drawn ratios of EFA fibers (Figure 14(b)). The linearity of changes in crystallinity of drawn fiber well-corresponds to dependency of WAXD (110) intensity on drawing (Figure 12(b)). Further, from the qualitative estimation of the lamella thickness based on the crystallization degree, the thickness of the crystalline regions of the EFA lamella form was estimated to vary within a range from 6 to 16 nm (Figure 14(c)). In the case of DR5 fiber with most superior transmission ability of infrared light, almost 50% crystallinity and 11 nm lamella thickness are estimated. Therefore, it seems that the enhancement of transmission ability is not caused by increases of crystallinity, but reducing of differences in density between crystal and amorphous region. Probably, a high light transmission rate is not brought about by formation of extreme homogeneous crystalline fiber, but by formation of like a "fringed micelle-type" lamella arrangement which has an indistinct lamella-interface based on the enhancement of density for amorphous parts by drawing. In the case over six times drawing, since transition from amorphous part to crystalline part occurrs in EFA fiber, the density reduction of amorphous region and increases of differences in density between crystal and amorphous parts have developed. As a result, it seems that the transmission ability of infrared light decreases over six times drawing to EFA fibers.

Figure 15 shows the schematic illustrations of the hierarchical structures ranging from the lamellae on the nanometer scale to the crystal structure on the subnanometer scale of a transparent EFA fiber.[44] We suggested that the crystal structure of the crystalline fluorinated polymers such as PTFE, EFA, PFA, and

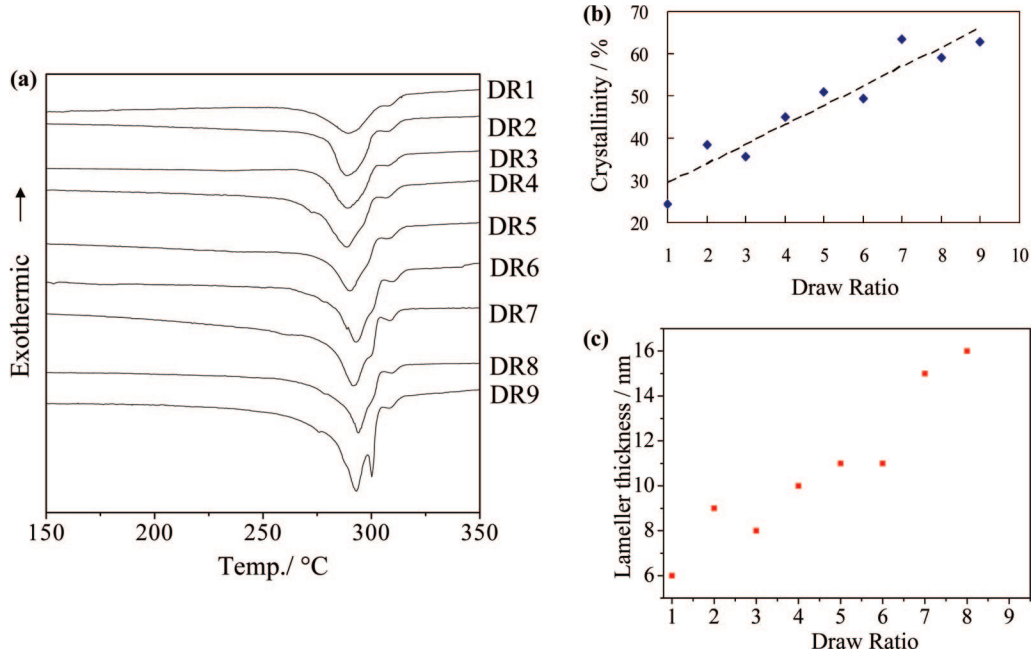

Figure 14. (a) DSC thermograms of drawn EFA fibers at several ratios (scanning rate, 10 °C min^{-1}). (b) Plot of drawn ratio vs crystallinity of drawn EFA fibers at several ratios. (c) Plot of lamellar thickness vs crystallinity of drawn EFA fibers at several ratios.

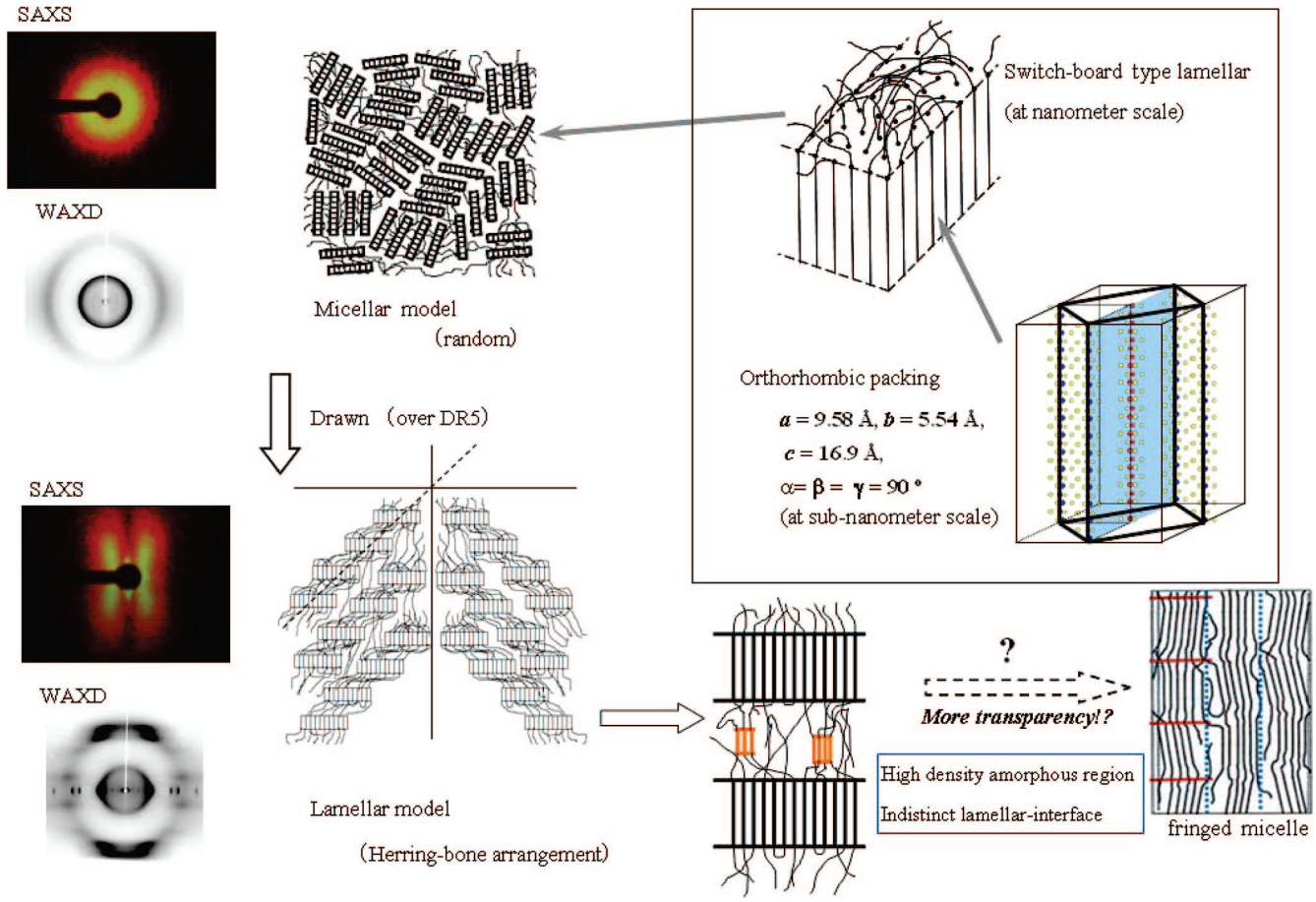

Figure 15. Schematic illustrations of hierarchical structure in EFA transparent fiber at the range from lamella arrangement on a few ten nanometer scale to crystal structure on the subnanometer scale.

so on, form the orthorhombic system. At the nanometer scale, undrawn EFA fiber forms an isotropic random micellar texture at room temperature. The lamella in "crystalline" transparent fiber of EFA forms a "herringbone" arrangement when it was drawn over five times. In the view of transparency, we suggest that differences in density between crystal and amorphous region are extremely small as a negligible quantity at this drawn ratio. The crystalline fluorinated copolymer like EFA also formed lamella crystal and spherulites.[25] Further, from the results of WAXD in this study, crystallite sizes themselves in the fiber are unchanged with drawn ratios (Figure 12(b)). Therefore, the experimental facts of changes in "nontransparency of unprocessed fluorinated polymer", "semitransparency of undrawn fiber", and "increases of transparency with drawn ratios" are not able to explain by only logic of formation of fine structure less sized than the wavelength of visible and infrared light.

It is suggest that increases in transparency are brought about by formation of like a "fringed micelle-type" lamella arrangement which have indistinct lamella-interface based on the increase of density for amorphous parts by drawing. Upon further drawing, the density in the crystal region increased and in the amorphous region decreased (Figure 14(c)) gradually although the overall differences in electron density between the crystalline and the amorphous regions estimated by SAXS were almost invariable (Figure 6(b)). Probably, the progression of further transparency and the ability of light conductivity were brought about by a formation of indistinct lamellar-interface with small difference of densities as a negligible quantity. As an ideal type of extremely transparent crystalline fiber, the formation of a fringed micelle-type lamella arrangement with high density of amorphous region like crystal and indistinct lamellar-interface may be desirable because of the low differences in densities inside the fibers.

4. Conclusion

The changes in fine structure upon drawing transparent crystalline EFA fibers were investigated by WAXD and SAXS measurements. EFA was crystallized as a lamella crystal in the fibers although the polytetrafluoroethylene homopolymer itself usually forms extended-chain crystals. EFA exhibited thicker lamellae (thickness: at least 27 nm) as observed by the SAXS measurement. In this type of crystalline fluorinated copolymers, we considered the formation of a switchboard-type lamella model according to Flory's suggestion. With an increase in the drawing of the fibers, four-point SAXS diagrams developed in the photograph of EFA transparent fibers, which implied that a particular type of layer structure, the alternately tilted lamella arrangement known as the herringbone, was formed. Furthermore, it was found that the previously proposed packing mode of general fluorinated polymers was required to be reconsidered from quasi-hexagonal to orthorhombic in a reciprocal lattice in order to assign all the reflective indexes obtained by using high-resolution WAXD measurements. Furthermore, the orientation of the crystallite and the elongation of lamella of EFA were completed simultaneously in the drawn fibers. The quasi-crystallization process progressed upon further drawing up to five times. After that, an increase in the density of the amorphous region and a partial appearance of voids probably occurred simultaneously. The crystalline EFA fiber at DR5 exhibited excellent transparency and infrared light conductivity. The light transmission property was related closely to the lamella ar-

rangement, crystal structure, and difference in the crystalline/amorphous density of crystalline EFA fibers.

References and Notes

(1) Keller, A. *Philos. Mag.* **1957**, *2*, 1171.
(2) Till, P. H. *J. Polym. Sci.* **1957**, *24*, 301.
(3) Fischer, E. W. *Z. Naturforsch.* **1957**, *12* (a), 753.
(4) Bu, H. S.; Pang, Y. W.; Song, D. D.; Yu, T. Y.; Voll, T. M.; Czornyj, G.; Wunderlich, B. *J. Polym. Sci., Part B: Polym. Phys.* **1991**, *29*, 139.
(5) Lotz, B.; Mathieu, C.; Thierry, A.; Lovinger, A. J.; De Rosa, C.; de Ballesteros, O. R.; Auriemma, F. *Macromolecules* **1998**, *31*, 9253.
(6) Burdon, J.; Tatlow, J. C. *Advances in Fluorine Chemistry*; Stacey, M., Tatlow, J. C., Sharp, A. G., Eds.; Academic Press: New York, 1960; Vol. *1*, pp 129−165.
(7) Patrick, C. R.; Stacey, M.; Tatlow, J. C.; Sharpe, A. G. *Advances in Fluorine Chemistry*; Butterworths Publications Ltd.: London, 1961; Vol. *2*, pp 1−34.
(8) Fluoropolymers 2. In *Topics in Applied Chemistry*; Hougham, G., et al., Eds.; Kluwer Acad./Plenum Pub.: New York, 1999.
(9) Symons, N. K. J. *J. Polym. Sci., A* **1963**, *1*, 2843.
(10) Rahl, R. J.; Evanco, M. A.; Frendericks, R. J.; Reimschuessel, A. C. *J. Polym. Sci. A-2* **1972**, *1*, 1337.
(11) Ozawa, T. *Bull. Chem. Soc. Jpn.* **1984**, *57*, 952.
(12) Marega, C.; Marigo, A.; Causin, V.; Kapeliouchko, V.; Nicoló, E. D.; Sanguineti, A. *Macromolecules* **2004**, *37*, 5630.
(13) Marega, C.; Marigo, A.; Garbuglio, C.; Fichera, A.; Martorana, A.; Zannetti, R. *Macromol. Chem.* **1989**, *190*, 1425.
(14) Marega, C.; Marigo, A.; Cingano, G.; Zannetti, R.; Paganetto, G. *Polymer* **1996**, *37* (25), 5549.
(15) Lee, J. C.; Namura, S.; Kondo, S.; Abe, A. *Polymer* **2001**, *42*, 8631.
(16) Overney, R. M.; Meyer, E.; Frommer, J.; Brodbeck, D.; Luthi, R.; Howald, L.; Güntherodt, H. J.; Fujihira, M.; Takano, H.; Gotoh, Y. *Nature* **1992**, *359*, 133.
(17) Overney, R. M.; Meyer, E.; Frommer, J.; Güntherodt, H. J. *Langmuir* **1994**, *10*, 1281.
(18) Fujimori, A.; Shibasaki, Y.; Araki, T.; Nakahara, H. *Macromol. Chem. Phys.* **2004**, *205*, 843.
(19) Fujimori, A.; Araki, T.; Nakahara, H. *Chem. Lett.* **2000**, 898.
(20) Bunn, C. W.; Howells, E. R. *Nature* **1954**, *18*, 549.
(21) Koike, Y. *Polymer* **1991**, *32*, 1737.
(22) Koike, Y.; Naritomi, M. Japan Patent 3719733, US Patent 5,783,636, EU Patent 0710855, KR Patent 375581, CN Patent ZL 951903152, TW Patent 090942, **1994**.
(23) Ishigure, T.; Kano, M.; Koike, Y. *J. Lightwave Technol.* **2000**, *18*, 178.
(24) Nam, P. H.; Ninomiya, N.; Fujimori, A.; Masuko, T. *Polym. Eng. Sci.* **2006**, *46* (6), 703.
(25) Fujimori, A.; Hasegawa, M.; Masuko, T. *Polym. Int.* **2007**, *56*, 1281.
(26) Flory, P. J. *J. Am. Chem. Soc.* **1962**, *84*, 2857.
(27) Salem, D. R.; Moore, R. A. F.; Weigmann, H. D. *J. Polym. Sci., Part B: Polym. Phys.* **1987**, *25*, 567.
(28) Salem, D. R. *Polymer* **1992**, *33*, 3182.
(29) Vasanthan, N.; Salem, D. R. *J. Polym. Sci., Part B: Polym. Phys.* **2001**, *39* (5), 536.
(30) Tanaka, K.; Seto, T.; Hara, T.; Tajima, Y. *Rep. Prog. Polym. Phys. Jpn.* **1964**, *7*, 63.
(31) Hinrichsen, G. *Angew. Makromol. Chem.* **1971**, *20* (1), 121.
(32) Harburn, G.; Lewis, J. W.; Warwicker, J. O. *Polymer* **1985**, *26*, 469.
(33) Kaji, K.; Mochizuki, T.; Akiyama, A.; Hosemann, R. *J. Mater. Sci.* **1978**, *13*, 972.
(34) Samuels, R. J. *J. Macromol. Sci.* **1970**, *701*, 241.
(35) Butler, M. F.; Donald, A. N. *J. Appl. Polym. Sci.* **1998**, *67*, 321.
(36) Stribeck, N.; Sapoundjieva, D.; Denchev, Z.; Apostolov, A. A.; Zachmann, H. G.; Stamm, M.; Fakirov, S. *Macromolecules* **1997**, *30*, 1339.
(37) Hernández; J., J.; Gracía-Gutiérrez, M. C.; Nogals, A.; Rueda, D. R.; Sanz, A.; Sics, I; Hsiao, B. S.; Roslaniec, Z.; Broza, G.; Ezquerra, T. A. *Polymer* **2007**, *48*, 3286.
(38) Sperati, C. A.; Starkweather, H. W., Jr *Adv. Polym. Sci.* **1961**, *2*, 465.
(39) Bunn, C. W.; Cobbold, A. J.; Palmer, R. P. *J. Polym. Sci.* **1958**, *19*, 365.
(40) (a) Clark, E. S; Muus, L. T. *Z. Kristallogr.* **1962**, *117*, 119. (b) Clark, E. S.; Muus, L. T. *Z. Kristallogr.* **1962**, *117*, 108.
(41) Klug, H. P.; Alexander, L. E. *X-ray Diffraction Procedures*; John Wiley and Sons: New York, 1974.
(42) (a) Hermans, P. H.; Platzek, P. *Kolloid Z.* **1939**, *88*, 68. (b) Hermans, J. J.; Hermans, P. H.; Vermaas, D.; Weidinger, A. *Recl. Trav. Chim. Pays-Bas* **1946**, *65*, 427.
(43) Wilchinsky, Z. W. *J. Appl. Phys.* **1959**, *30*, 792.
(44) Hayasaka, Y.; Fujimori, A. *Trans. Mater. Res. Soc. Jpn.* **2008**, *33*, 86.

MA800801D